Atmos. Chem. Phys. Discuss., 6, 2923–2964, 2006
www.atmos-chem-phys-discuss.net/6/2923/2006/

Atmospheric Chemistry and Physics Discussions

Application of thermal dissociation-laser induced fluorescence (TD-LIF) to measurement of HNO_3, Σalkyl nitrates, Σperoxy nitrates, and NO_2 fluxes using eddy covariance

D. K. Farmer[1], **P. J. Wooldridge**[1], **and R. C. Cohen**[1,2]

[1]Department of Chemistry; University of California, Berkeley, CA, 94720, USA
[2]Dept. of Earth and Planetary Science; University of California, Berkeley, CA, 94720, USA

Received: 22 December 2005 – Accepted: 17 January 2006 – Published: 12 April 2006

Correspondence to: R. C. Cohen (rccohen@berkeley.edu)

Abstract

Nitrogen exchange between the atmosphere and biosphere directly influences atmospheric composition. While much is known about mechanisms of NO and N_2O emissions, instrumentation for the study of mechanisms contributing to exchange of other major nitrogen species is quite limited. Here we describe the application of a new technique, thermal dissociation-laser induced fluorescence (TD-LIF), to eddy covariance measurements of the fluxes of NO_2, total peroxy acyl and peroxy nitrates, total alkyl and multifunctional alkyl nitrates, and nitric acid. The technique offers the potential for investigating mechanisms of exchange of these species at the canopy scale over timescales from days to years. Examples of flux measurements at a ponderosa pine plantation in the mid-elevation Sierra Nevada Mountains in California are reported and used to evaluate instrument performance.

1 Introduction

The exchange of nitrogen between the biosphere and atmosphere affects both oxidative atmospheric chemistry and ecosystem nutrient dynamics, with potential indirect effects on the carbon cycle and climate (Vitousek et al., 1997; Ollinger et al., 2002). Nitrogen enters ecosystems through either biotic nitrogen fixation of N_2 or atmospheric deposition of gaseous or particulate ammonium and oxidized nitrogen, is rapidly cycled in both organic and inorganic forms, and is known to be released from ecosystems to the atmosphere through direct plant emissions of NO or NO_2, and as a by-product of soil microbial transformations, namely as NO or N_2O via nitrification and denitrification. As N is commonly the limiting nutrient for plant growth in forest ecosystems, increased N deposition also increases carbon uptake (Vitousek et al., 1997). This effect has clear implications as the CO_2 level in the atmosphere continues to rise concurrently with increased anthropogenic N emission and consequent increased N deposition to ecosystems (Sievering et al., 2001). However, because N emissions contribute to

ACPD

6, 2923–2964, 2006

ozone formation, increased N deposition associated with those emissions may also be accompanied by increased deposition of ozone. The negative impact of ozone on plant health may offset the positive effects of N deposition on C uptake (Ollinger et al., 2002). The continued increase in anthropogenic emissions of reactive nitrogen into the atmosphere and thus nitrogen deposition has lead to concerns regarding nitrogen saturation, which may decrease plant health, increase greenhouse gas emissions, and affect water quality (Aber et al., 1998).

Bulk wet and dry nitrate/ammonium deposition has been quantified over numerous ecosystems (e.g. Bytnerowicz et al., 1996; Holland et al., 2005 and references therein). More detailed experiments have focused on NO and N_2O because of their clear soil sources, the greenhouse warming potential of N_2O, and the availability of commercial detectors (e.g. Hanson et al., 1991; Davidson et al., 1997; Ludwig et al., 2001; Mosier et al., 2004 and references therein). However, ammonia (NH_3) and the reactive nitrogen oxides (NO_y=NO+NO_2+PAN + other peroxy nitrates + alkyl nitrates + nitric acid + N_2O_5 + . . .) are significant contributors to N dry deposition, and recent research indicates that surface interactions affect atmospheric concentrations and partitioning of these species. For example, extreme changes in the atmospheric reactive nitrogen budget following biomass burning or rain events have been observed (Zhang et al., 2002; Jaegle et al., 2004; Bertram et al., 2006). Few studies have investigated the magnitude and mechanisms of ecosystem-scale exchange of NO_2, peroxy nitrates, alkyl nitrates or HNO_3, likely because of the absence of techniques for measurement of these reactive nitrogen oxide species with both adequate sensitivity and minimal day-to-day maintenance requirements to enable application to ecosystem-scale flux measurements. Eddy covariance (EC) is the most direct method of measuring the exchange of compounds between the atmosphere and earth's surface (Dabberdt et al., 1993). This technique has stringent requirements for measurements of vertical wind speed and concentration, requiring observations that are fast (>1 Hz), sensitive, portable, and free of interferences (Baldocchi et al., 1988; McMillen, 1988). EC flux measurements of NO_y, NO, and NO_2 fluxes have been reported (e.g. Delany

ACPD
6, 2923–2964, 2006

EGU

et al., 1986; Munger et al., 1996; Rummel et al., 2002; Horii et al., 2004). Most other studies of N fluxes have used enclosure or indirect estimation techniques, including gradient measurements or resistance modeling (Hanson et al., 1991; Wesely et al., 2000).

The most extensive measurements are those described by Munger et al. (1996), who observed NO_y using eddy covariance at both remote ($0.5\,\mu mol\,m^{-2}\,h^{-1}$ summertime net dry NO_y flux, Schefferville, Quebec) and rural ($3.4\,\mu mol\,m^{-2}\,h^{-1}$ summertime, $3.2\,\mu mol\,m^{-2}\,h^{-1}$ wintertime, Harvard Forest) environments. Munger et al. (1998) modeled that deposition of hydroxyalkyl nitrates, HNO_3 from heterogeneous reactions of N_2O_5 and HNO_3 from oxidation of NO_2 by OH contributed comparably to total NO_y deposition during summer at Harvard Forest. Horri (2002) found that while the NO_y flux at Harvard Forest was explained by HNO_3 deposition with minor NO_2 and PAN contributions for unpolluted background flows, up to 50% of the NO_y flux in polluted flows was not accounted for by NO_2, PAN, and HNO_3, and was therefore likely due to alkyl or hydroxyalkyl nitrates and other peroxy or peroxy acyl nitrates.

All published HNO_3 flux measurements have been either inferential (e.g. Lefer et al., 1999; Tarnay et al., 2001) or indirect (e.g. Huebert et al., 1988; Janson et al., 1999; Pryor et al., 2002; Nemitz et al., 2004). Tarnay et al. (2001) used inferential flux measurements at Lake Tahoe, CA, and determined that dry deposition of HNO_3 is the major source of atmospheric N to the lake. HNO_3 deposition velocities of $7.6\,cm\,s^{-1}$ were measured at Niwot Ridge using the flux gradient approach (Sievering et al., 2001). Pryor et al. (2002) used both gradient and relaxed eddy accumulation (REA) techniques to measure HNO_3 fluxes. While downward fluxes were generally observed, Pryor et al. (2002) also observed HNO_3 efflux, potentially due to a chemical flux divergence involving HNO_3-NH_3-NH_4NO_3 reactions and gas-particle nitrate partitioning.

The sum of multifunctional and alkyl nitrates (ΣANs), compounds with the formula $RONO_2$ where R is any organic functional group, have recently been shown to constitute a significant fraction of atmospheric reactive nitrogen (Day et al., 2003; Rosen et al., 2004; Cleary et al., 2005). Total peroxy acyl and peroxy nitrates (ΣPNs, compounds

with the formula RO_2NO_2 (peroxy nitrates) or $RC(O)O_2NO_2$ (peroxy acyl nitrates)) and ΣANs may include hydroxyl substituted species that are highly soluble in water, and are thus likely to strongly interact with the biosphere. Leaf-scale studies demonstrated that plants can directly uptake peroxyacetyl nitrate (PAN), demonstrating a mechanism for dry deposition of PAN (Sparks et al., 2003; Teklemariam et al., 2004). Laboratory measurements have demonstrated that uptake of PAN by an alfalfa canopy occurs with a deposition velocity of 0.75 cm s^{-1} (Hill, 1971). However, observational evidence for strong daytime PAN deposition on an ecosystem scale is equivocal. For example, Doskey et al. (2004) used the modified Bowen ratio technique to measure daytime PAN deposition velocities over a grassland site; while upward PAN fluxes were observed during sunny afternoons, possibly due to chemistry associated with emission of precursor compounds, net PAN fluxes averaged over three months were downward with an average deposition velocity of 0.13±0.13 cm s^{-1}. Nighttime velocity measurements using ^{222}Radon and PAN concentrations showed significant, though variable, deposition (Schrimpf et al., 1996), as had been indicated by previous studies (Shepson et al., 1992). The potential for exchange of organic nitrates between ecosystems and the atmosphere is particularly important to consider more carefully following research suggesting that organic nitrates play an important role in ecosystem nutrient cycling (Neff et al., 2002; Perakis et al., 2002; Bragazza et al., 2004).

While NO is generally observed to be emitted from soils (e.g. Gasche et al., 2002; Rummel et al., 2002; Jaegle et al., 2004), both emission and deposition of NO_2 have been observed using eddy covariance over grasslands and fields (Wesely et al., 1982; Delany et al., 1986). At Harvard Forest, Horii observed downward NO fluxes and upward NO_2 fluxes (Horii, 2002). NO_x fluxes are complicated by rapid within-canopy radical reactions that occur on a chemical timescale faster than that of the physical exchange, i.e. flux divergence (Vila-Guerau de Arellano et al., 1993). Following emission from soils, NO reacts with O_3 to produce NO_2, thus decreasing the observed NO upward flux, and potentially causing a net upward NO_2 flux. Thus there is the potential for within-canopy oxidation, measurement height above the canopy, and other factors

affecting canopy and atmospheric NO_x levels to affect the observed NO, NO_2 and O_3 fluxes. This flux divergence has been observed in an Amazonian rain forest, where NO emissions from the soil were observed near the surface, but were not significant above the canopy (Rummel et al., 2002). NO_x fluxes are further complicated by direct leaf exchange that may lead to the presence of a compensation point. A compensation point is the atmospheric mixing ratio above which a compound is deposited and below which the compound is emitted. Compensation points for NO_2 of 0.53–1.60 ppb were reported for different plant species by Sparks et al. (2001).

Here we present the application of thermal dissociation – laser induced fluorescence (TD-LIF), a new technique for measuring mixing ratios of NO_2, total peroxy nitrates (ΣPNs), total alkyl and multifunctional alkyl nitrates (ΣANs), and HNO_3 (Day et al., 2002), to eddy covariance measurements. We evaluate the performance of the instrument based on field experiments at a mid-elevation ponderosa pine plantation in the Sierra Nevada Mountains and describe some of the observations.

2 Site

Field measurements were made in summer and fall of 2003 (June–November) and from the summer 2004 through spring of 2005 (May 2004–June 2005) above a ponderosa pine plantation planted in 1990 in the mid-elevation (1315 m) Sierra Nevada Mountains. The trees were about 9 m tall in 2004. The plantation is owned by Sierra Pacific Industries and is near the University of California at Berkeley's Blodgett Forest Research Station (UC-BFRS, 38°53′42.9″ N, 120°3757.9″ W) (see Goldstein et al., 2000 for complete description). The inlets and sonic anemometer were located ∼12 m above the ground on a walk-up tower, and ∼3 m above the top of the canopy; the TD-LIF detector is located in a temperature-controlled shed located just north-east of the tower. The site is characterized by a Mediterranean climate with a cold, wet season (October-April) and a warm, dry season (May–September). In the summer, daytime winds are predominantly southwest (210–240°), upslope from the Sacramento Valley.

Nighttime winds are from the northeast (30°), downslope from the Sierra Nevada. A diesel generator provides power to the site, and is located ~130 m to the north of the tower.

3 Instrumentation

Measurements of NO_2, ΣPNs, ΣANs, and HNO_3 were made with the Berkeley thermal dissociation-laser induced fluorescence instrument (TD-LIF) (Thornton et al., 2000; Day et al., 2002). Briefly, air is pulled simultaneously through a single inlet manifold into four channels, each of which consists of an inlet, heated section of quartz tube ("oven") and LIF NO_2 detector. Each class of compounds (ΣPNs, ΣANs, HNO_3) thermally dissociates to NO_2 and an accompanying radical (RO_2, RO, OH) at a characteristic temperature. The ovens are separately thermostatted at 550°C, 330°C, 180°C, and ambient temperature (Day et al., 2002). At 180°C, ΣPNs dissociate to NO_2 and the signal in that channel is the sum of NO_2+ΣPNs. The 330°C channel adds ΣANs, and the 550°C channel HNO_3 to the total. Mixing ratios of each class (ΣPNs, ΣANs, and HNO_3) are the difference in NO_2 observed in channels set at adjacent temperatures; for example, the difference in NO_2 detected in the 330°C channel and 180°C channel is the ΣANs mixing ratio. No filters were placed in front of the inlet, thus both gaseous and particulate NO_y compounds may be measured. Bertram and Cohen (2003) demonstrated evaporation and detection of semi-volatile NH_4NO_3 aerosol to NO_2 in the 550°C channel and that non-volatile aerosols (e.g. $NaNO_3$) are not detected; semi-volatile organic nitrate aerosols are expected to evaporate and be detected in the 330°C oven. Thus our reported HNO_3 is the sum of gas and semi-volatile aerosol N and our ΣANs are the sum of gas and semi-volatile aerosol ΣANs.

Our technique for LIF detection of NO_2 is described in detail in Thornton et al. (2000) and Day et al. (2002). Briefly, a custom-built, tunable dye laser is pumped at 8 kHz by a compact, diode-pumped, Q-switched frequency-doubled Nd^{3+}-YAG laser (Spectra Physics, average power of 3 W at 532 nm, 30 ns pulse length). The dye laser

ACPD
6, 2923–2964, 2006

EGU

(pyrromethene-597 in isopropanol) emits a 25-ns wide (FWHM) pulse at 585 nm (linewidth 0.06 cm^{-1}), and is tuned to a specific, narrow rovibronic feature of NO_2. The dye laser tuning is alternated between this strong NO_2 resonance and a weaker continuum absorption to test for interferences, assess background scatter, and maintain a frequency-lock on the spectral feature of interest. The instrument chop cycle is maintained at 20 s on-resonance, followed by 5 s off-resonance. The laser light is focused through each of four multipass (White) cells in series. We collect the red-shifted (>700 nm) fluorescence photons with cooled GaAs photomultiplier tubes (Hamamatsu H7421-50) using time-gated single-photon counting. The fluorescence signal, collected at 5 Hz, is directly proportional to the NO_2 mixing ratio. The cell pressure is reduced to ~3 Torr using a roots blower (Eaton M-62 supercharger) backed by an oil-sealed rotary vane pump. These pumps maintain a flow of ~1500 sccm through each of the four cells (total flow of 6000 sccm).

Comparisons between the TD-LIF and independent measurement techniques demonstrate the ability of TD-LIF to adequately measure NO_{yi}. Thornton et al. (2003) showed that the daily average agreement between NO_2 mixing ratios observed by photolysis to NO followed by chemiluminescence (PCL) and LIF was better than 5% in Nashville, TN during the 1999 Southern Oxidant Study and again outside of Houston during TEXAQS-2000. Comparisons between the $\sum$PNs measured by TD-LIF and $\sum PAN_i$ (=PAN + PPN + PiBN + MPAN + APAN) measured by GC-ECD during the TexAQS-2000 study in LaPorte, TX showed agreement within 6% (Rosen, 2004). NO_y measured by chemiluminescence was on average within 1% during the daytime with $\sum NO_{yi}$ (=NO_2 (TD-LIF) + $\sum$PNs (TD-LIF) + $\sum$ANs(TD-LIF) + HNO_3(TD-LIF) + HONO (DOAS) + NO_3(DOAS) + NO (CL) + $NO^-_{3\,aerosol}$(PILS)) during the TexAQS-2000 campaign (Rosen, 2004).

We define the sensitivity of this NO_2 measurement technique as that mixing ratio for which the signal to noise for a given averaging time is equal to 2. Thus the sensitivity depends on the calibration constant and background signal rate, which vary with laser

ACPD
6, 2923–2964, 2006

power and cell alignment. The NO_2 signal is calculated as

$$S_{NO2}=S_{total}-B\,, \quad (1)$$

where S_{NO2} is the NO_2 signal, S_{total} is the total LIF counts measured during the experiment and B is the background, or mean of LIF counts measured in zero air. Because the background signal is obtained from an average over several minutes, random error in B is negligible compared to errors in S_{total}, which is obtained over 0.2 s. The noise in the NO_2 signal is given by Poisson statistics as $\sqrt{S_{total}}$, or $\sqrt{S_{NO2}+B}$. Over the course of the campaign described here, the sensitivity ranged from 24 pptv in 0.2 s to 64 pptv in 0.2 s due to degradation of laser performance. Maintenance was performed every 4–7 days to optimize the sensitivity. As described in Day et al. (2002), because each class of compounds is calculated as the difference in signals observed in adjacent cells, the uncertainty for each compound is a function of both instrument sensitivity and mixing ratios measured in adjacent channels:

$$(S_A - S_B) \pm (\Delta_A^2 + \Delta_B^2)^{1/2} \quad (2)$$

where S_A and S_B are the signals from adjacent channels, and Δ_A and Δ_B are their associated uncertainties, as calculated above for NO_2. The instrument's sensitivity to the difference in adjacent channels, e.g. for ΣPNs, is calculated considering $S/N=2=(S_A-S_B)/(\Delta_A^2+\Delta_B^2)^{1/2}$. For typical background counts and calibration constants, the sensitivity for ΣPNs above a 1-ppb background of NO_2 is 66 ppt in 0.2 s.

As HNO_3 adsorbs strongly even to Teflon surfaces at ambient temperatures and humidities (e.g. Neuman et al., 1999), a fast response inlet was designed to minimize HNO_3 loss before air enters the two hot ovens (550°C, 330°C). This inlet was also designed to minimize dust and prevent insects from entering the sampling lines. The fore region of the inlet, which allows the addition of calibration and zero flows, is made of extruded PFA (perfluroalkoxy) Teflon tubing and injection-molded compression PFA fittings (Swagelok). Hot processed (extruded or molded) parts appear to be significantly better than those machined from PFA bar stock, presumably because hot processing

ACPD
6, 2923–2964, 2006

leaves a smoother, more closed surface. To minimize the losses at high relative humidity, most of the inlet plumbing is thermostatted at 60°C, a temperature high enough to prevent HNO_3 wall loss, but low enough to prevent unintended dissociation of ΣPNs during the transit time. The inlet manifold is designed to minimize flow distortion, to ensure that flows are identical, and to maintain identical inlet residence times for all four channels. The manifold consists of two identical 1″-diameter short tubes, which draw air into the fore region in which air is sub-sampled and split into one of two adjacent ovens. The two outer tubes are vertically displaced by 5 cm, and are placed ~20 cm behind the sonic anemometer in the prevailing daytime wind direction. The heater sections are 25–30 cm long and 0.4 mm I.D. quartz; the quartz continues for another 60–80 cm to allow the gas to cool before reaching the junction to the PFA tubing (~18 m) that carries the NO_2 product to the detection cells. A pressure-reducing orifice is incorporated into this junction, decreasing the pressure and shortening the transit time from the inlet.

We characterized the time responses for HNO_3 and n-propyl nitrate by spiking concentrated samples in front of the inlet and monitoring the resulting signal (Fig. 2). The primary time constants for the rise and fall for both species are ≤0.6 s, though a low-amplitude secondary decay with a time constant of ~7 s was observed for HNO_3, but not n-propyl nitrate. As these measurements were spikes to laboratory air (containing 30–40 ppbv NO_y, relative humidity ~30%), the HNO_3 and n-propyl nitrate released remained in the laboratory, causing non-zero background mixing ratios after the spikes.

A sonic anemometer (Campbell Scientific CSAT3 3-D Sonic Anemometer) located on the tower, pointing into the daytime wind direction, at the same height and <30 cm in front of the TD-LIF inlet, measures wind speed in three dimensions (sample rate of 5 Hz), allowing for wind direction and virtual temperature to be calculated.

ACPD
6, 2923–2964, 2006

4 Data processing

Fluorescence collected by the PMTs was converted to mixing ratio using a standard calibration procedure (Day et al., 2002). Each step in this procedure was reinvestigated in detail to check that it did not produce unintended contributions to the flux. Briefly, data were normalized to the running mean of the entrance laser power for each cell, as observed separately for the on and off-resonance measurements. The line-locking protocol varies the dye-laser frequency about the center of the NO_2 absorption peak. The maximum absorbance is observed to coincide with the maximum fluorescence and we correct the fluorescence signal by comparing the on-resonance absorbance to the local maximum in absorbance measured through the NO_2 reference cell.

Background counts due to chamber scatter, PMT dark noise, and any residual NO_2 in the system, were measured by overflowing the inlet with zero air (Sabio, Model 1001 Portable Air Source) for 170 s at 30-min intervals. Background counts for the ambient channel were typically <5 counts per second (cps), or ~40 ppt NO_2. The instrument was calibrated every 2 h with an NO_2 standard (NIST-traceable 4.77 ppm NO_2 (±5%) with 0.2 ppm NO in N_2, Praxair CA) diluted to 1–10 ppb in zero air. The calibration standard was compared to other NIST-traceable NO_2 standards in our lab at least once a year, and was found to be stable in NO_2 mixing ratio. The calibration mixture was transported in separate lines from the pure zero air to prevent residual NO_2 from affecting background measurements, and was introduced as an overflow at the inlet so that it passes through the ovens and sampling lines before being detected. The mixing ratio data were corrected (<5%) for quenching by water (Thornton et al., 2000).

Spikes in NO_x caused by the diesel generator are occasionally observed during periods of light, variable winds, most often at night. Data influenced by spikes were identified and removed by first flagging data points in which NO_2 or NO_y varied by more than 5 standard deviations from the mean for a given half hour, and then by removing any remaining spikes by hand.

Data from the sonic anemometer were processed by rotating the wind vectors for

ACPD
6, 2923–2964, 2006

each half hour to ensure that the vertical wind measurements were taken normal to the shear plane (Baldocchi et al., 1988, McMillen, 1988). Data from the sonic anemometer and the LIF system are acquired at the same rate (5 Hz) and on the same computer using programs that run independently. Nonetheless, the data points do not necessarily coincide exactly in time, and may be shifted by <0.2 s. To correct for this problem, we linearly interpolate the LIF data onto the sonic anemometer time stamp prior to flux analysis.

The finite length of tubing between the inlet at the top of the tower and the LIF detection sensor on the ground causes a time lag in measurements taken by the sonic and TD-LIF systems. This time lag is the sum of time taken for a given parcel of air to move past the sonic anemometer and into the inlet, which is a function of wind speed and distance between the inlet and anemometer, plus the time taken for the air to move from the inlet into the LIF chamber, which is a function of tube length and pumping speed. The pumping speed varied daily with air density, which depends on atmospheric pressure and temperature. However, the effect of these variations on lag time was minor (<0.5 s), and did not affect observed fluxes. While the length of sample tubing was roughly the same for each sample line, slight differences in the pinhole size for each sampling line and the arrangement of vacuum tubing from the Roots blower to the LIF chambers caused the pressure in each chamber to be slightly different (between 2.7 and 3.1 Torr). This lagtime is accounted for in the EC analysis by calculating the covariance between measurements from the sonic and LIF detector with varying lagtimes and subtracting the appropriate lag. A peak in these lagged covariance plots occurs at the lagtime required for the sample air to move through the sample tubing (Fig. 3). The maximum covariance observed in a lagged covariance plot for mixing ratio and vertical wind speed is the EC flux. For example, on 28 September 2004, the lag peaked at 3 s for the 550°C channel, 2.6 s for the 330 and 180°C channels, and 1.6 s for the ambient NO_2 channel; the ordering of these lagtimes was coincidental. As expected, no lagtime is observed between the vertical wind speed and temperature as the vertical wind speed and virtual temperature are derived from measurements

ACPD
6, 2923–2964, 2006

taken on the same instrument.

5 Mixing ratios

NO_y mixing ratios at UC-BFRS are between 0.5–3 ppb and exhibit a diurnal trend of increasing mixing ratio with the upslope wind during the day, maximizing in the late evening, and decreasing when the downslope flows return cleaner air until late morning (Dillon et al., 2002; Day, 2003). Unlike other rural sites, NO_y maxima in the summer are higher than in the winter (Day, 2003). We attribute this to stronger transport from urban source areas during summer. During the study period, NO_x mixing ratios range from 0.2 to 1.0 ppb; ΣPNs from 0.1 to 1.0 ppb; ΣANs from 0.05 to 0.5 ppb, and HNO_3 from 0.01 ppb to 1.0 ppb. Ozone mixing ratios ranged from 35 to 70 ppb. Mid-day ozone fluxes are about 45–50 μmol m^{-2} h^{-1} in the summer, and 15 μmol m^{-2} h^{-1} in the winter (Kurpius et al., 2003). Figure 1 shows the median mixing ratios of NO_2, ΣPNs, ΣANs and HNO_3 versus time of day.

6 Eddy covariance fluxes

The EC flux for a given species, F_c, is calculated as the covariance between the vertical wind speed and species mixing ratio,

$$F_c = \frac{1}{n}\sum_{i=1}^{n}(w_i - \bar{w})\cdot(c_i - \bar{c}), \quad (3)$$

where n is the number of points used for the calculation, w_i and c_i are instantaneous measurements of vertical wind speed and mixing ratio, and $\bar{w}$ and $\bar{c}$ are the mean vertical wind speed and mixing ratio respectively. A positive flux indicates upwards movement of mass from the surface to the atmosphere. Measurements are typically taken for ~30 min at 5 Hz, which is both long and fast enough to capture all flux-carrying

ACPD
6, 2923–2964, 2006

eddies. Fluxes measured by the EC method are valid only if the assumptions behind Taylor's "frozen flow" hypothesis are met, namely that eddies move past the tower unchanged and in stationary flow (Stull, 1988).

The eddy covariance technique requires that the calculated fluxes do not vary within time-scales of analysis, the stationarity requirement. We tested for stationarity by comparing the 30-minute flux $\langle w'c' \rangle_{30\,\mathrm{min}}$ to the mean of fluxes calculated from the six consecutive 5-min samples within the half hour, $\overline{\langle w'c' \rangle_{5\,\mathrm{min}}}$. Data for which the ratio of sub-set flux mean to half-hour mean was not within ±30% (Geissbuhler et al., 2000),

$$0.7 < \frac{\overline{\langle w'c' \rangle_{5\,\mathrm{min}}}}{\langle w'c' \rangle_{30\,\mathrm{min}}} < 1.3\,, \tag{4}$$

were assumed to be non-stationary. More than 95% of the previously filtered $NO_{y,i}$ data from the winter season (January–March 2005) were stationary. The sensible heat fluxes are not filtered for spikes due to the nearby generator prior to analysis, and only met the stationarity criterion for 67% during winter 2005. For September 2004, more than 93% of $NO_{y,i}$ data not influenced by the generator were stationary, while 66% of the sensible heat data were stationary. Most of the non-stationary sensible heat fluxes were at times when spikes from the generator were observed.

Nighttime EC CO_2 fluxes are typically filtered to exclude data observed in low turbulence regimes, as determined by a threshold friction velocity ranging from 0.0 to 0.6 m s^{-1} (Massman et al., 2002). These filters are often applied when CO_2 fluxes correlate with friction velocity at low u*, which should not occur because CO_2 fluxes are assumed to be driven by biological controls, and thus uncorrelated to turbulence (Massman et al., 2002). However, as the controlling mechanisms of NO_{yi} fluxes are poorly understood, there is no clear evidence that the fluxes are biologically determined. Thus we have not removed nighttime data that has passed the stationarity test, although nighttime u* at Blodgett Forest ranged from 0.01 to 0.5 m s^{-1} during September 2004. Future work will analyze the long-term NO_{yi} flux dataset from Blodgett to determine whether a u* threshold should be applied.

As fluxes are calculated from the deviations from the mean for a given scalar, a time-varying mean mixing ratio causes spurious fluxes. We used a 10-minute running mean to calculate the perturbations from the mean for scalar mixing ratio and vertical wind speed, c' and w'. The turbulent flux for a given half hour is the average of the product of these two values, $<c'w'>$ (McMillen, 1988). Sensitivity tests determined that the 10-min running mean was long enough to capture trends caused by movement of pollutant plumes and chemical changes; inspection of cospectra (see below) show that the low frequency eddies that are removed using 10-min means were not important to the total flux. Similar to mixing ratio measurements, fluxes were determined for each of the four channels, and the difference between adjacent channels gives the flux for each class. This is theoretically identical to calculating fluxes by taking the difference between appropriately lagged channels, and calculating the flux for each class of species. The theoretical conclusion was borne out in practice, as identical fluxes were calculated either way {i.e., $F(NO_{2(T2)}–NO_{2(T1)})=F(NO_{2(T2)})–F(NO_{2(T1)})$} where $NO_{2(T)}$ refers to the total NO_2 observed at a particular oven temperature. No density corrections are required for the eddy flux measurements as the TD-LIF measures the mixing ratio of a species in the atmosphere rather than the absolute concentration (Webb et al., 1980). All mixing ratio and flux analysis programs were written specifically for this instrument.

7 Spectral analysis

EC measurements are known to be challenging because of the wide dynamic range in frequency required of the sensors. We test the TD-LIF fluxes using a variety of spectral analyses that demonstrate the experimental capabilities. Figures 3 and 4 show mean mixing ratios and fluxes for summer 2004 (June–August). Eddy covariance fluxes are potentially subject to underestimation by systematic errors due to 1) time lags between the sonic anemometer and mixing ratio measurements, 2) separation between the sonic anemometer and inlet, and 3) damping of high frequency fluctuations. Time lags between mixing ratio and wind measurements are accounted for as described

ACPD
6, 2923–2964, 2006

above. The magnitude of underestimation of fluxes due to the separation distance between the sonic anemometer and the chemical inlet depends on the mean wind speed. The flux underestimation can be calculated for lateral (perpendicular to wind direction) and longitudinal (parallel to wind direction) separation using a spectral transfer function (Moore, 1986):

$$T_s(f) = e^{-9.9f^{1.5}} \quad (5)$$

where $f = \frac{n \cdot s}{\overline{U}}$ is the normalized frequency for which the function is being calculated, n is frequency (Hz), s is the separation distance (m), and $\overline{U}$ is the mean wind speed ($m\,s^{-1}$). The lateral separation between the TD-LIF inlets and sonic anemometer is <5 cm, and results in a negligible effect on the flux; a 5-cm separation and mean wind speeds of 0.5, 1.5, 5, and 10 $m\,s^{-1}$ correspond to underestimation by 1.82, 0.22, 0.03, and 0.01%. The longitudinal separation is ~20 cm. A 20-cm separation distance and mean wind speeds of 0.5, 1, 2, 5, and 10 $m\,s^{-1}$ cause underestimation by 99.3%, 20.1%, 1.82%, 0.25%, and <0.1%. For median daytime windspeeds of 3 $m\,s^{-1}$ this effect is an error of less than 1%. At night when wind speeds are typically 1 $m\,s^{-1}$, this effect can cause as much as 20% attenuation of the flux. However, Moore (1986) points out that this transfer function does not consider wind direction and likely overestimates the loss. We ignore flow distortion due to the inlet and sonic anemometer as the anemometer is faced into the prevailing daytime wind direction. The title angle is the angle required to rotate the sonic anemometer vectors about the horizontal axis to give a mean vertical wind speed of zero, and provides an indication of flow distortion (Goulden et al., 1996). The tilt angle for 30-min intervals is always less than 10° from zero, and indicates only minor flow distortion from either tower shadowing or the inlet set up (McMillen, 1988). The 3.69° (0.03=standard deviation from the mean, N=3023) tilt angle for winds in the 200–360° (SSW-N) direction (1 July 2004 to 30 November 2004), which account for over 75% of daytime winds, has little variability demonstrating negligible flow distortion for daytime winds over the fetch. The variability in tilt angle is greater in the 100–150° wind directions (–1.3°, σ=0.06, N=2821), demonstrating that passing through the tower

(NE-SE winds) affects turbulence. Nighttime fluxes will be more significantly impacted, as only ∼35% of the winds originate in the 200–360° direction. As the variance in tilt angle in the prevailing wind direction is relatively small, the inlet design likely does not cause significant flow distortion.

When fluids pass through long sample tubes, the high frequency fluctuations are dampened by smearing due to the different speeds traveled by fluctuations being carried at different frequencies, or spectral attenuation (Lenschow et al., 1991). We calculate the half-power fluctuation damping frequency of the sample tubing (1/8″ I.D.) according to Lenschow and Raupach (1991); this is the frequency at which half the spectral power is lost due to attenuation. The half-power damping frequency is ∼6 Hz for our system. Damping at this frequency will result in minimal attenuation of NO_{yi} fluxes as cospectra show that most of the NO_{yi} flux is carried by turbulence occurring on significantly slower timescales. A spectral correction may be applied to data to account for this dampening effect on observable fluctuations. One commonly used correction technique is to apply a transfer function to the cospectra to determine the fractional error of the measured flux, and to account for signal loss (Moore, 1986; Massman, 1991). Application of Massman's transfer function to typical cospectra from our dataset demonstrates that under most circumstances <2% of the flux is lost due to spectral attenuation. In rare circumstances when the calculated lagtimes indicate a slower flow through the tubing, losses as high as 7% are calculated.

Power spectra of both the observed vertical wind speed and LIF mixing ratio data are level at the low frequencies (0.02 Hz), showing that the measurement interval of 30 min is long enough to capture the low frequency eddies that carry flux (Fig. 5a). The spectrum for only one channel is presented because all four channels have very similar spectra, as expected for identical inlet configurations and detection techniques. The power spectra have $(\text{frequency})^{-5/3}$ behavior for frequencies between 0.02 and 0.8 Hz, indicative of the inertial subrange and demonstrating that the TD-LIF sensitivity is adequate to measure mixing ratio perturbations due to turbulence (Anderson et al., 1986). At frequencies greater than ∼1 Hz the mixing ratio power spectra become noise

ACPD
6, 2923–2964, 2006

EGU

limited as indicated by the rapid fall off in spectral density.

Cospectra of vertical wind speed and temperature and vertical wind speed and mixing ratio both show the same slopes, and both deviate from the expected (frequency)$^{-7/3}$ slope in the same way (Fig. 5b). This behavior is characteristic of the inertial subrange between 0.01–0.8 Hz. Again, all four channels produce similar logarithmic cospectra. The slopes for both TD-LIF and sonic anemometer cospectra are more shallow than the –7/3 slope expected from Komolgorov theory, which can not be due to spectral attenuation, as this should not occur in the sensible heat cospectra. The –7/3 slope is predicted from dimensional analysis, and deviations are not unprecedented. In long-term studies of turbulence spectra over two mixed hardwood forests, Su et al. (2004) observed turbulence spectra with shallower slopes in the inertial subrange than the expected. Blanken et al. (1998) similarly observed cospectral slopes in the inertial subrange less than theoretically expected for fluxes of sensible heat, water and CO_2 both above and below a boreal aspen forest. The shallow cospectra slopes observed in this study suggest that the cascade of energy transfer from larger to smaller eddies in the inertial subrange occurs with a power law smaller than the –7/3 suggested by dimensional analysis. The cospectra on a semi-logarithmic scale (Fig. 6) further demonstrate that the main contributions to flux are from eddies in the 0.01- to 0.5-Hz frequency range (corresponding to 6–300 m horizontally for a 3 m s^{-1} wind) (Kaimal et al., 1972; Anderson et al., 1986). This frequency range is similar to the 0.005 to 0.5 Hz range observed for NO_y by Munger et al. (1996), and confirms that the TD-LIF time response is adequate. The structure observed within the TD-LIF cospectra can be removed by averaging data in larger frequency bins, but is potentially indicative of complex process controlling NO_{yi} fluxes, and was thus preserved in Fig. 5. The data also confirm that measurements with characteristic time constants significantly shorter than the maximum 0.6 s TD-LIF time constant would have been of limited additional benefit. Loss of flux signal from the instrument time constant can be

approximated as:

$$\frac{F_m}{F_t} = \frac{1}{(1 + 2\pi f_m \tau)} \quad (6)$$

where F_m is the observed flux, F_t is the true flux, f_m is the frequency at which the frequency-multiplied cospectrum maximizes, and τ is the first-order response time of the sensor (Horst, 1997). For f_m of 0.01 Hz and τ of 0.6 s, the underestimation is 3.6% for the HNO_3 flux. As these are conservative estimates of f_m and τ, we do not correct for this underestimation in the fluxes presented in Fig. 4.

To test for interferences and prevent drift of the laser frequency, the TD-LIF measurement algorithm alternates the laser frequency on and off the NO_2 resonance in a 25-second cycle. However, imperfections in the instrument calibration at the on and off resonance frequencies will introduce fluctuations at 25 s (0.04 Hz), which could potentially covary with fluctuations in the vertical wind speed, causing spurious fluxes. The power spectra (e.g. Fig. 7a) show a clear, narrow peak at 0.04 Hz, as well as the harmonics of this signal at 0.08, 0.12, and 0.16 Hz (marked with stars). The cospectra of mixing ratio and vertical wind speed (Fig. 7b) still have peaks at 0.04 Hz and its harmonics, but they are dampened because the chop cycle is independent of fluctuations in the vertical wind speed. The potential effect of the chop cycle on fluxes was quantified by integrating the area under the semi-log cospectrum in the frequency regions affected by the chop cycle and determined to be negligible (<1%).

The LIF-vertical wind speed cospectra are less coherent than the sensible heat cospectra derived solely from the sonic anemometer (Fig. 5b). The high-frequency ($\geq$1 Hz) noise is possibly due to higher instrument noise in the LIF detector than the sonic anemometer. The variations at lower frequencies for the mixing ratio cospectra are more likely due to chemical reactions and the fact that production and deposition of certain species is inhomogeneous within the fetch, causing varying mixing ratios in the horizontal plane, thus affecting observed fluxes and cospectra (Delany et al., 1986). Future studies will include a more thorough analysis of these variations.

ACPD
6, 2923–2964, 2006

Instrument noise may correlate with vertical wind speed resulting in a spurious flux, contributing to uncertainty in the observed scalar flux. We determine this uncertainty both theoretically and experimentally. The contribution to flux variance due to instrument noise, $\sigma^2_{inst}(F;T)$, can be written as

$$\sigma^2_{inst}(F;T) = \frac{\sigma^2_w \sigma^2_n \Delta t}{T}, \quad (7)$$

where σ^2_w and σ^2_n are the variance in vertical wind speed ($m^2\,s^{-2}$) and instrument noise (ppb^2) respectively, Δt is the sampling interval (0.2 s for 5-Hz measurements), and T is the averaging time (s) (Lenschow et al., 1985; Ritter et al., 1990). As the instrument noise is dominated by shot noise, the variance in instrument noise can be calculated for each half hour sampling interval as the square root of the total number of photon counts, converted to mixing ratio units by the appropriate calibration constant. The photon counts vary with scalar mixing ratio and laser alignment within each White cell. The calculated contribution to error in the measured fluxes from instrument counting noise is calculated as the square root of σ^2_{inst}. For example, for typical noon-time σ^2_w of $0.7\,m^2\,s^{-2}$ and instrument shot noise of 0.01 ppb, the $\sigma^2_{inst}(F;T)$ is $7.78\times10^{-9}\,ppb^2\,m^2\,s^{-2}$, causing an uncertainty of $8.8\times10^{-5}\,ppb\,m\,s^{-1}$ ($0.013\,\mu mol\,m^{-2}\,h^{-1}$) for a half hour of 5-Hz data. On a typical day the average uncertainty in the flux ranged from $1.38\times10^{-6}\,ppb\,m\,s^{-1}$ for the 550°C channel to $2.86\times10^{-5}\,ppb\,m\,s^{-1}$ for NO_2. These calculated contributions to error in the measured fluxes are orders of magnitude less than the measurements. The contribution to flux uncertainty for ΣPNs, ΣANs and HNO_3 is calculated by propagation of the contributions from adjacent channels. For example, the error for fluxes centered around noon of 10 September 2004, a typical summer day, are calculated to be 7.03×10^{-5}, 3.65×10^{-5} and $1.44\times10^{-5}\,ppb\,m\,s^{-1}$ for ΣPNs, ΣANs, and HNO_3, respectively.

Zero-air measurements provide experimental validation that TD-LIF fluxes are not dominated by instrument noise. Zero air was flowed into the inlet continuously for ~30 min in the morning of 10 September 2004, and the observed LIF signals in each

channel were combined with sonic anemometer data to calculate a zero-air flux. Because TD-LIF measurement rely on differences between the channels there might be additional contributions to the error budget of a measurement associated with imperfect subtraction that are not captured by these zero air fluxes. However we have found no evidence for such effects. The zero air fluxes are single-point measurements of instrument noise to flux. Because the variance is the integral of a power spectrum, comparison of the power spectra of a half-hour of zero air (Fig. 7a, grey) to a half hour of ΣNO_{yi} (Fig. 7a, black) demonstrates that the variance in measured ΣNO_{yi} is minimally affected by variance in instrument noise. The cospectrum of instrument noise (Fig. 8) is completely flat with a maximum amplitude of 0.008 ppb m s^{-1} independent of frequency, compared to typical mixing ratio fluxes (Fig. 5b) which exhibit an inertial sub-range. We calculated fluxes from the half-hour of measurements of zero-air with 30-min intervals of vertical wind speed data following protocols identical to our EC flux calculations for atmospheric data. The maximum and minimum noise flux for 10 September 2004 were 3.83×10^{-4} and 1.28×10^{-6} ppb m s^{-1} for the 550°C channel, and 4.6×10^{-3} and 5.91×10^{-6} ppb m s^{-1} for the ambient NO_2 channel. For the differences between channels we observe maximum zero air fluxes of 6.3×10^{-5}, 7.5×10^{-3}, and 1.2×10^{-3} ppb m s^{-1} and minimum fluxes of 6.3×10^{-5}, 5.8×10^{-6}, and 6.9×10^{-7} ppb m s^{-1} for ΣPNs, ΣANs, and HNO_3. For reasons we cannot fully explain, these measurements are an order of magnitude larger than the error calculated using Eq. (7), though they are still small compared to the measured fluxes. As an example, Table 1 compares observed fluxes with theoretical and experimental estimates of noise for the half-hour at noon on 10 September 2004.

These zero fluxes can be used to estimate a minimum observable flux using the TD-LIF method of subtracting adjacent channels. As fluxes for ΣPNs, ΣANs, and HNO_3 are calculated as a difference in fluxes of adjacent channels (F_{diff}), we can consider the flux measurement sensitivity due to instrument noise similarly to the above calculations

of the random component of uncertainties and sensitivities in mixing ratio data:

$$F_{diff}=F_A-F_B \pm \left(\Delta_{Fa}^2+\Delta_{Fb}^2\right)^{1/2} \quad (8)$$

For 10 September 2004, with a S/N=2=$F_A-F_B/(\Delta_{Fa}^2+\Delta_{Fb}^2)^{1/2}$, where Δ_{Fa} and $\Delta_{Fb}=1.55\times10^{-5}$ and 1.063×10^{-4} ppb m s^{-1} for the HNO_3 channel, we calculate that $|F_A-F_B|\geq2.15\times10^{-4}$ ppb m s^{-1} (0.0316 μmol m^{-2} h^{-1}) will have S/N>2. Similarly, the minimum observable flux is 2.16×10^{-4} and 6.03×10^{-4} ppb m s^{-1} for ΣANs and ΣPNs respectively. While it is difficult to generalize this estimate of a detection limit because it depends both on the instrument sensitivity and on the variance of the vertical winds, we do find that daytime fluxes are almost always a factor of 10–100 larger than the uncertainty estimated from the zero air measurement, and that nighttime fluxes when $u^*<0.1$ m s^{-1} may sometimes have signal to noise less than 2.

8 Patterns in the fluxes

The fluxes and mixing ratios observed at Blodgett Forest represent a large and complex dataset that will be discussed in detail in future manuscripts.

The mean winter fluxes (Fig. 9) demonstrate the potential of the TD-LIF method when coupled to EC. Winter-time ΣNO_{yi} fluxes are dominated by midday deposition of Σ peroxy nitrates, Σ alkyl nitrates and HNO_3, while NO_2 exhibits a variable, if slightly upward, flux (Fig. 4). The net downward flux of ΣANs and ΣPNs flux is a sign of the potentially important role of deposition of these organic nitrogen species to the forest ecosystem during winter. Upward NO_2 fluxes may be due to a combination of several processes. As the NO_2 mixing ratios are low, a compensation point may cause plants within the ecosystem to release NO_2, as observed on the leaf scale for tropical plants (Sparks et al., 2001). As the ground was covered by snow during the winter, a direct release of NO_2 as a result of snow photochemistry could also cause emission (Domine et al., 2002). A third mechanism potentially responsible for the upward NO_2

fluxes is emission of NO, either from plants (Wildt et al., 1997) or snow (Domine et al., 2002), followed by reaction with O_3 in the canopy, resulting in a net observed upward flux. Fluxes of all species are significantly smaller at nighttime than daytime, likely due to the low turbulence (friction velocity <0.17 m s^{-1}) and significant attenuation. As the nighttime wind direction is in the opposite direction from the sonic anemometer, air may have to pass through the tower before reaching the inlet and anemometer, potentially causing perturbations to the turbulence and removing the stickier HNO_3 and hydroxyl-alkyl nitrates.

During the winter, mixing ratios of ΣNO_y are lower than in the summer (Figs. 3, 9). Regional winds in the winter are weaker, preventing the Sacramento air plume from reaching Blodgett Forest much of the time. The variability in mixing ratio likely contributes to the variability in observed deposition. By normalizing the flux by mixing ratio, we can obtain the deposition velocity, V_{dep}:

$$V_{dep} = \frac{-F}{C} \quad (9)$$

where F is the flux and C is the mixing ratio. The median V_{dep} for HNO_3 during winter afternoons between 11:00–13:00 PST was 2.52 cm s^{-1}, and 80% of the data fall between V_{dep} of –1.23 and 8.17 cm s^{-1}. For ΣANs the median V_{dep} was 2.05 cm s^{-1}, and 80% fell in the range 1.34 to 18.14 cm s^{-1}, while for ΣPNs the median V_{dep} was 0.84 cm s^{-1}, and the 80% range is –0.57 to 6.26 cm s^{-1}.

The net exchange of ΣNO_{yi} over a given period can be derived by integrating the total flux over the time period of interest. Unfortunately, generator failures and instrumental problems at Blodgett Forest occurred throughout the winter, and resulted in a patchy dataset that included only a third of the winter days (1 January 2005–31 March 2005). To determine the net exchange, we integrated the average winter diurnal cycle of ΣNO_{yi} fluxes, and multiplied by 90 days. Assuming that the median winter cycle adequately represents the winter exchange, Blodgett Forest experiences 0.102 kgN ha^{-1} dry ΣNO_y deposition in the winter. No measurements of dry deposition have been

ACPD
6, 2923–2964, 2006

made at UC-BFRS, though estimates of summer deposition fluxes to Ponderosa pines at Whitaker's Forest, which is south of UC-BFRS, from a foliage rinsing technique estimated annual dry deposition of 1.0–1.5 kgN ha^{-1} (Bytnerowicz et al., 1995). Other studies suggest the Sierra Nevada receives an average of 1.7 kgN ha^{-1} yr^{-1} wet deposition (Bytnerowicz et al., 1996). Measurements at Lake Tahoe, which is higher in elevation and further east than Blodgett, indicate summertime dry deposition ranging from 1.2-8.6 kgN ha^{-1} yr^{-1} for the summer and fall, versus wet deposition, which ranges from 1.7 to 2.9 kgN ha^{-1} yr^{-1} (Tarnay et al., 2001). The TD-LIF-derived estimate of dry deposition of NO_{yi} species during the winter at Blodgett Forest is lower than total N deposition measurements elsewhere in the Sierra Nevada, likely because of higher HNO_3 mixing ratios in the summer and high HNO_3 mixing ratios closer to direct NO_x sources in California's Central Valley or from tourism within the Lake Tahoe basin.

Mean summer fluxes (Fig. 4) are characterized by upward fluxes in NO_2, ΣPNs, and HNO_3, and downward fluxes of ΣANs. The net upward NO_2, ΣPNs and HNO_3 fluxes suggest that within canopy chemistry competes with deposition for these reactive nitrogen oxides. The NO_2 observations are consistent with previous studies of O_3 at Blodgett Forest, which indicate chemical fluxes of O_3 due to reactions with NO emitted from soil microbial processes (Kurpius et al., 2003). The upward fluxes of ΣPNs and HNO_3 are likely due to within-canopy production following reaction of NO_2 with OH and $RC(O)O_2$ radicals produced during VOC oxidation. OH mixing ratios within the canopy at Blodgett Forest have been estimated as between $0.8–3\times10^7$ molecules cm^{-3} as a result of oxidation of VOCs by O_3 (Goldstein et al., 2004). We speculate that these high OH mixing ratios are adequate to produce enough within-canopy HNO_3 to affect the observed fluxes. Similarly the OH may affect ΣANs and ΣPNs through various chemical cycles. These data give a hint of the enormous potential for mechanistic studies of factors controlling N fluxes and processing of N by and within forest canopies that EC with TD-LIF provides.

ACPD
6, 2923–2964, 2006

9 Conclusions

We describe the application of TD-LIF for measuring eddy covariance fluxes of NO_2, ΣPNs, ΣANs, and HNO_3. Spectral analysis of the data demonstrate that the TD-LIF measurements have the necessary time response and sensitivity to measure fluxes by eddy covariance, and that internal diagnostics and line locking procedures do not compromise the flux measurements. We evaluated sources of random error and possible biases in TD-LIF flux measurements; these are summarized in Table 2. Sensor separation, spectral attenuation in sample tubing, and instrument time response combine to produce a bias of less than 3.5% underestimation of daytime fluxes under typical atmospheric conditions. The laser chop cycle may contribute as much as a 1% random error. Both theoretical and experimental treatments of the contribution of instrument noise to flux error demonstrate that observed fluxes are not dominated by instrument noise. Zero air fluxes suggest that instrument noise typically contributes a random error of much less than 10% of the observed fluxes.

Initial observations at Blodgett Forest demonstrate that TD-LIF has the potential to shed light on the complexity of ecosystem-level exchange of the reactive nitrogen oxides. Winter fluxes at Blodgett Forest are dominated by deposition of HNO_3, ΣANs and ΣPNs. Within-canopy chemistry and the more complex factors controlling summer fluxes will be the subject of further study.

Acknowledgements. This research was supported by the NSF Atmospheric Chemistry Program under grant ATM-0138669. We gratefully acknowledge D. Day, E. Conlisk and I. Faloona for their contributions in the early stages of this project. Special thanks to the staff at UC-BFRS, in particular S. and D. Rambeau, for exceptional logistical support.

References

Aber, J., McDowell, W., Nadelhoffer, K., Magill, A., Berntson, G., Kamakea, M., McNulty, S., Currie, W., Rustad, L., and Fernandez, I.: Nitrogen saturation in temperate forest ecosys-

tems: Hypotheses revisited, BioScience, 48, 921–934, 1998.
Anderson, D. E., Verma, S. B., Clement, R. J., Baldocchi, D. D., and Matt, D. R.: Turbulence spectra of CO_2, water vapor, temperature, and velocity over a deciduous forest, Agricultural and Forest Meteorology, 38, 81–99, 1986.
Baldocchi, D. D., Hicks, B. B., and Meyers, T. P.: Measuring biosphere-atmosphere exchanges of biologically related gases with micrometeorological methods, Ecology, 69, 1331–1340, 1988.
Bertram, T. H. and Cohen, R. C.: A prototype instrument for the detection of semi-volatile organic and inorganic nitrate aerosol, Eos Trans. AGU, 84(46), Fall Meet. Suppl., Abstract A51F-0740, 2003.
Bertram, T. H., Heckel, A., Richter, A., Burrows, J. P., and Cohen, R. C.: Satellite meaurements of daily variations in soil NOx emissions, Geophys. Res. Lett., 32, in press, 2006.
Blanken, P. D., Black, T. A., Neumann, H. H., Den Hartog, G., Yang, P. C., Nesic, Z., Staebler, R., Chen, W., and Novak, M. D.: Turbulent flux measurements above and below the overstory of a boreal aspen forest, Boundary-Layer Meteorology, 89, 109–140, 1998.
Bragazza, L. and Limpens, J.: Dissolved organic nitrogen dominates in European bogs under increasing atmospheric N deposition, Global Biogeochemical Cycles, 18, GB4018, doi:10.1029/2004GB002267, 2004.
Bytnerowicz, A. and Riechers, G.: Nitrogenous Air-Pollutants in a Mixed-Conifer Stand of the Western Sierra-Nevada, California, Atmospheric Environment, 29, 1369–1377, 1995.
Bytnerowicz, A. and Fenn, M. E.: Nitrogen deposition in California forests: A review, Environmental Pollution, 92, 127–146, 1996.
Cleary, P. A., Murphy, J. G., Wooldridge, P. J., Day, D. A., Millet, D. B., McKay, M., Goldstein, A. H., and Cohen, R. C.: Observations of total alkyl nitrates within the Sacramento Urban Plume, Atmos. Chem. Phys. Discuss., 5, 4801–4843, 2005.
Dabberdt, W. F., Lenschow, D. H., Horst, T. W., Zimmerman, P. R., Oncley, S. P., and Delany, A. C.: Atmosphere-surface exchange measurements, Science, 260, 1472–1481, 1993.
Davidson, E. A. and Kingerlee, W.: A global inventory of nitric oxide emissions from soils, Nutrient Cycling in Agroecosystems, 49, 37–50, 1997.
Day, D. A., Wooldridge, P. J., Dillon, M. B., Thornton, J. A. and Cohen, R. C.: A thermal dissociation laser-induced fluorescence instrument for in situ detection of NO_2, peroxy nitrates, alkyl nitrates, and HNO_3, J. Geophys. Res., 107, 4046, doi:10.1029/2001JD000779, 2002.
Day, D. A., Dillon, M. B., Wooldridge, P. J., Thornton, J. A., Rosen, R. S., Wood, E. C., and

Cohen, R. C.: On alkyl nitrates, O_3, and the 'missing NO_y', J. Geophys. Res., 108, 4501, doi:10.1029/2003JD003685, 2003.
Delany, A. C., Fitzjarrald, D. R., Lenschow, D. H., Pearson Jr., R., Wendel, G. J., and Woodruff, B.: Direct measurements of nitrogen oxides and ozone fluxes over grassland, Journal of Atmospheric Chemistry, 4, 429–444, 1986.
Dillon, M. B., Lamanna, M. S., Schade, G. W., Goldstein, A. H., and Cohen, R. C.: Chemical evolution of the Sacramento urban plume: Transport and oxidation, J. Geophys. Res., 107, 4045, doi:10.1029/2001JD000969, 2002.
Domine, F., and Shepson, P. B.: Air-snow interactions and atmospheric chemistry, Science, 297, 1506–1510, 2002.
Doskey, P. V., Kotamarthi, V. R., Fukui, Y., Cook, D. R., Breiteil III, F. W., and Wesely, M. L.: Air-surface exchange of peroxyacetyl nitrate at a grassland site, J. Geophys. Res., 109, D10310, doi:10.1029/2004JD004533, 2004.
Gasche, R. and Papen, H.: Spatial variability of NO and NO_2 flux rates from soil of spruce and beech forest ecosystems, Plant and Soil, 240, 67–76, 2002.
Geissbuhler, P., Siegwolf, R., and Eugster, W.: Eddy covariance measurements on mountain slopes: The advantage of surface-normal sensor orientation over a vertical set-up, Boundary-Layer Meteorology, 96, 371–392, 2000.
Goldstein, A. H., Hultman, N. E., Fracheboud, J. M., Bauer, M. R., Panek, J. A., Xu, M., Wi, Y., Guenther, A. B., and Baugh, W.: Effects of climate variability on the carbon dioxide, water and sensible heat fluxes above a ponderosa pine plantation in the Sierra Nevada (CA), Agricultural and Forest Meteorology, 101, 113–129, 2000.
Goldstein, A. H., McKay, M., Kurpius, M. R., Schade, G. W., Lee, A., Holzinger, R., and Rasmussen, R. A.: Forest thinning experiment confirms ozone deposition to forest canopy is dominated by reaction with biogenic VOCs, Geophys. Res. Lett., 31, L22106. doi:10.1029/2004GL021259, 2004.
Goulden, M. L., Munger, J. W., Fan, S. M., Daube, B. C., and Wofsy, S. C.: Measurements of carbon sequestration by long-term eddy covariance: Methods and a critical evaluation of accuracy, Global Change Biology, 2, 169–182, 1996.
Hanson, P. J. and Lindberg, S. E.: Dry deposition of reactive nitrogen compounds: A review of leaf, canopy and non-foliar measurements, Atmospheric Environment, 25A, 1615–1634, 1991.
Hill, A. C.: Vegetation – Sink for Atmospheric Pollutants, J. Air Pollut. Control Assoc., 21, 341–

346, 1971.
Holland, E. A., Braswell, B. H., Sulzman, J., and Lamarque, J.-F.: Nitrogen deposition onto the United States and Western Europe: Synthesis of observations and models, Ecological Applications, 15, 38–57, 2005.
Horii, C. V., Munger, J. W., Wofsy, S. C., Zahniser, M., Nelson, D., and McManus, J. B.: Fluxes of nitrogen oxides over a temperate deciduous forest, J. Geophys. Res., 109, D08305, doi:10.1029/2003JD004326, 2004.
Horst, T. W.: A simple formula for attenuation of eddy fluxes measured with first-order-response scalar sensors, Boundary-Layer Meteorology, 82, 219–233, 1997.
Huebert, B. J., Luke, W. T., Delany, A. C., and Brost, R. A.: Measurements of concentrations and dry surface fluxes of atmospheric nitrates in the presence of ammonia, J. Geophys. Res., 93, 7127–7136, 1988.
Jaegle, L., Martin, R. V., Chance, K., Steinberger, L., Kurosu, T. P., Jacob, D. J., Modi, A. I., Yoboue, V., Sigha-Nkamdjou, L., and Galy-Lacaux, C.: Satellite mapping of rain-induced nitric oxide emissions from soils, J. Geophys. Res., 109, D21310, doi:10.1029/2004JD004787, 2004.
Janson, R. and Granat, L.: A foliar rinse study of the dry deposition of nitric acid to a coniferous forest, Agricultural and Forest Meteorology, 98–99, 683–696, 1999.
Kaimal, J. C., Wyngaard, J. C., Izumi, Y., and Cote, O. R.: Spectral characteristics of surface-layer turbulence, Q. J. R. Meteo., 98, 563–589, 1972.
Kurpius, M. R. and Goldstein, A. H.: Gas-phase chemistry dominates O_3 loss to a forest, implying a source of aerosols and hydroxyl radicals to the atmosphere, Geophys. Res. Lett., 30, 1371–1375, doi:10.1029/2002GL016785, 2003.
Lefer, B. L., Talbot, R. W., and Munger, J. W.: Nitric acid and ammonia at a rural northeastern U.S. site, J. Geophys. Res., 104, 1645–1662, 1999.
Lenschow, D. H. and Kristensen, L.: Uncorrelated noise in turbulence measurements, Journal of Atmospheric and Oceanic Technology, 2, 68–81, 1985.
Lenschow, D. H. and Raupach, M. R.: The attenuation of fluctuations in scalar concentrations through sampling tubes, J. Geophys. Res., 96, 15 259–15 268, 1991.
Ludwig, J., Meixner, F. X., Vogel, B., and Forstner, J.: Soil-air exchange of nitric oxide: An overview of processes, environmental factors, and modeling studies, Biogeochemistry, 52, 225–257, 2001.
Massman, W. J.: The attenuation of concentration fluctuations in turbulent flow through a tube,

J. Geophys. Res., 96, 15 269–15 274, 1991.
Massman, W. J. and Lee, X.: Eddy covariance flux corrections and uncertainties in long-term studies of carbonand energy exchanges, Agricultural and Forest Meteorology, 113, 121–144, 2002.
McMillen, R. T.: An eddy correlation technique with extended applicability to non-simple terrain, Boundary-Layer Meteorology, 43, 231–245, 1988.
Moore, C. J.: Frequency response corrections for eddy correlation systems, Boundary-Layer Meteorology, 37, 17–36, 1986.
Mosier, A., Wassman, R., Verchot, L., King, J., and Palm, C.: Methane and nitrogen oxide fluxes in tropical agricultural soils: Sources, sinks and mechanisms, Environment, Development and Sustainability, 6, 11–49, 2004.
Munger, J. W., Wofsy, S. C., Bakwin, P. S., Fan, S.-M., Goulden, M. L., Daube, B. C., Goldstein, A. H., Moore, K. E., and Fitzjarrald, D. R.: Atmospheric deposition of reactive nitrogen oxides and ozone in a temperate deciduous forest and a subarctic woodland. 1. Measurements and mechanisms, J. Geophys. Res., 101, 12 639–12 657, 1996.
Munger, J. W., Fan, S.-M., Bakwin, P. S., Goulden, M. L., Goldstein, A. H., Colman, A. S., and Wofsy, S. C.: Regional budgets for nitrogen oxides from continental sources: Variations of rates for oxidation and deposition with season and distance from source regions, J. Geophys. Res., 103, 8355–8368, 1998.
Neff, J. C., Holland, E. A., Dentener, F. J., McDowell, W. H., and Russell, K. M.: The origin, composition and rates of organic nitrogen deposition: A missing piece of the nitrogen cycle?, Biogeochemistry, 57/58, 99–136, 2002.
Nemitz, E., Sutton, M. A., Wyers, G. P., and Jongejan, P. A. C.: Gas-particle interactions above a Dutch heathland: 1. Surface exchange fluxes of NH_3, SO_2, HNO_3 and HCl, Atmos. Chem. Phys., 4, 989–1005, 2004.
Neuman, J. A., Huey, L. G., Ryerson, T. B., and Fahey, D. W.: Study of inlet materials for sampling atmospheric nitric acid, Environmental Science and Technology, 33, 1133–1136, 1999.
Ollinger, S. V., Aber, J. D., Reich, P. B., and Freuder, R. J.: Interactive effects of nitrogen deposition, tropopheric ozone, elevated CO_2 and land use history on the carbon dynamics of northern hardwood forests, Global Change Biology, 8, 545–562, 2002.
Perakis, S. S. and Hedin, L. O.: Nitrogen loss from unpolluted South American forests via dissolved organic compounds, Nature, 415, 416–419, 2002.

Pryor, S. C., Barthelmie, R. J., Jensen, B., Jensen, N. O., and Sorensen, L. L.: HNO_3 fluxes to a deciduous forest derived using gradient and REA methods, Atmospheric Environment, 36, 5993–5999, 2002.

Ritter, J. A., Lenschow, D. H., Barrick, J. D. W., Gregory, G. L., Sachse, G. W., Hill, G. F., and Woerner, M. A.: Airborne flux measurements and budget estimates of trace species over the Amazon Basin during the GTE/ALBE 2B expedition, J. Geophys. Res., 95, 16 875–16 886, 1990.

Rosen, R. S., Wood, E. C., Wooldridge, P. J., Thornton, J. A., Day, D. A., Kuster, W., Williams, E. J., Jobson, B. T., and Cohen, R. C.: Observations of total alkyl nitrates during Texas Air Quality Study 2000: Implications for O_3 and alkyl nitrate photochemistry, J. Geophys. Res., 109, D07303, doi:10.1029/2003JD004227, 2004.

Rummel, U., Ammann, C., Gut, A., Meixner, G. X., and Andreae, M. O.: Eddy covariance measurements of nitric oxide flux within an Amazonian rain forest, J. Geophys. Res., 107, 8050, doi:10.1029/2001JD000520, 2002.

Schrimpf, W., Lienaerts, K., Muller, K. P., Rudolph, J., Neubert, R., Schubler, W., and Levin, I.: Dry deposition of peroxyacetyl nitrate (PAN): Determination of its deposition velocity at night from measurements of the atmopsheric PAN and ^{222}radon concentration gradient, Geophys. Res. Lett., 23, 3599–3602, 1996.

Shepson, P. B., Bottenheim, J. W., Hastie, D. R., and Venkatram, A.: Determination of the Relative Ozone and Pan Deposition Velocities at Night, Geophys. Res. Lett., 19, 1121–1124, 1992.

Sievering, H., Kelly, T., McConville, G., Seibold, C., and Turnipseed, A.: Nitric acid dry deposition to conifer forests: Niwot Ridge spruce-fir-pine study, Atmospheric Environment, 35, 3851–3869, 2001.

Sparks, J. P., Monson, R. K., Sparks, K. L., and Lerdau, M.: Leaf uptake of nitrogen dioxide (NO_2) in a tropical wet forest: implications for tropospheric chemistry, Oecologia, 127, 214–221, 2001.

Sparks, J. P., Roberts, M. J., and Monson, R. K.: The uptake of gaseous organic nitrogen by leaves: A significant global nitrogen transfer process, Geophys. Res. Lett., 30, 2189–2292, 2003.

Su, H. B., Schmid, H. P., Grimmond, C. S. B., Vogel, C. S., and Oliphant, A. J.: Spectral characteristics and correction of long-term eddy-covariance measurements over two mixed hardwood forests in non-flat terrain, Boundary-Layer Meteorology, 110, 213–253, 2004.

Tarnay, L., Gertler, A. W., Blank, R. R., and Taylor Jr., G. E.: Preliminary measurements of summer nitric acid and ammonia concentrations in the Lake Tahoe Basin air-shed: implications for dry deposition of atmospheric nitrogen, Environmental Pollution, 113, 145–153, 2001.

Teklemariam, T. A. and Sparks, J. P.: Gaseous fluxes of peroxyacetyl nitrate (PAN) into plant leaves, Plant, Cell and Environment, 27, 1149–1158, 2004.

Thornton, J. A., Wooldridge, P. J., and Cohen, R. C.: Atmospheric NO_2: In situ laser-induced fluorescence detection at parts per trillion mixing ratios, Analytical Chemistry, 72, 528–539, 2000.

Thornton, J. A., Wooldridge, P. J., Cohen, R. C., Williams, E. J., Hereid, D. P., Fehsenfeld, F. C., Stutz, J., and Alicke, B.: Comparisons of in situ and long path measurements of NO_2 in urban plumes, J. Geophys. Res., 108, 4496, doi:10.1029/2003JD003559, 2003.

Vila-Guerau de Arellano, J., Duynkerke, P. G., and Builtjes, P. J. H.: The divergence of the turbulent diffusion flux in the surface layer due to chemical reactions: the NO-O_3-NO_2 system, Tellus, 45B, 23–33, 1993.

Vitousek, P. M., Aber, J. D., Howarth, R. W., Likens, G. E., Matson, P. A., Schindler, D. W., Schlesinger, W. H., and Tilman, D. G.: Human alteration of the global nitrogen cycle: Sources and consequences, Ecological Applications, 7, 737–750, 1997.

Webb, E. K., Pearman, G. I., and Leuning, R.: Correction of flux measurements for density effects due to heat and water vapour transfer, Q. J. R. Meteo., 106, 85–100, 1980.

Wesely, M. L., Eastman, J. A., Stedman, D. H., and Yalvac, E. D.: An eddy-correlation measurement of NO_2 flux to vegetation and comparison to O_3 flux, Atmospheric Environment, 16, 815–820, 1982.

Wesely, M. L. and Hicks, B. B.: A review of the current status of knowledge on dry deposition, Atmospheric Environment, 34, 2261–2282, 2000.

Wildt, J., Kley, D., Rockel, A., Rockel, P., and Segschneider, H. J.: Emission of NO from several higher plant species, JGR, 102, 5919–5927, 1997.

Zhang, Q., Carroll, J. J., Dixon, A. J., and Anastasio, C.: Aircraft measurements of nitrogen and phosphorus in and around the Lake Tahoe Basin: Implications for possible sources of atmospheric pollutants to Lake Tahoe, Environmental Science and Technology, 36, 4981–9, 2002.

Table 1. Errors in eddy covariance fluxes from TD-LIF instrument noise from the half-hour centered around noon, 10 September 2004.

Channel	Observed Flux ($ppb\,m\,s^{-1}$)	Theoretical noise ($ppb\,m\,s^{-1}$) (relative error)	Zero air flux ($ppb\,m\,s^{-1}$) (relative error)
550°C (ΣNO_{yi})	0.0184	3.44×10^{-6} (0.02%)	1.50×10^{-5} (0.08%)
330°C ($\Sigma ANs + \Sigma PNs + NO_2$)	0.0173	1.40×10^{-5} (0.08%)	3.38×10^{-4} (1.95%)
180°C ($NO_2 + \Sigma PNs$)	0.0467	3.37×10^{-5} (0.07%)	-1.9×10^{-3} (4.1%)
Ambient (NO_2)	0.0196	6.17×10^{-5} (0.31%)	1.8×10^{-3} (9.2%)

ACPD
6, 2923–2964, 2006

Table 2. Summary of errors affecting TD-LIF eddy covariance fluxes, with conservative estimates of relative contribution to flux.

Source of Error	Bias	Relative error (1 m/s mean wind speed)	Relative error (5 m/s mean wind speed)	Error analysis reference
Sensor separation, lateral	Underestimate	<0.43%	<0.03%	Moore, 1986
Sensor separation, longitudinal	Underestimate	<20.2	<0.25%	Moore, 1986
Spectral attenuation	Underestimate	<7% (typically, <2%)		Lenschow and Raupach, 1991
Instrument time response	Underestimate	<3.6%		Horst, 1997
Chop cycle	None	<1%		this work
Instrument noise	None	<2%[a]		Lenschow and Kristensen, 1985; Ritter et al. 1990
Instrument noise	None	<15%[b]		this work

[a] For lowest instrument sensitivities kept in this dataset.
[b] For typical results by channel, see Table 1.

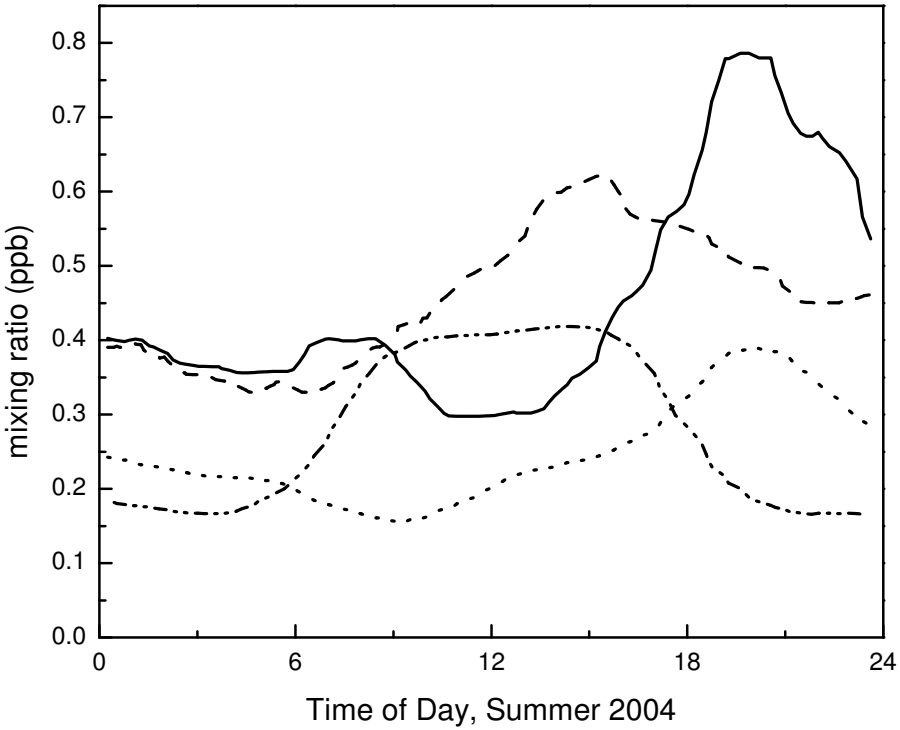

Fig. 1. Average mixing ratios (ppb) by time of day from August–September 2004 of NO_2 (⁻⁻⁻), total peroxy nitrates (—), total alkyl nitrates (•••), and HNO_3 (-••-).

ACPD
6, 2923–2964, 2006

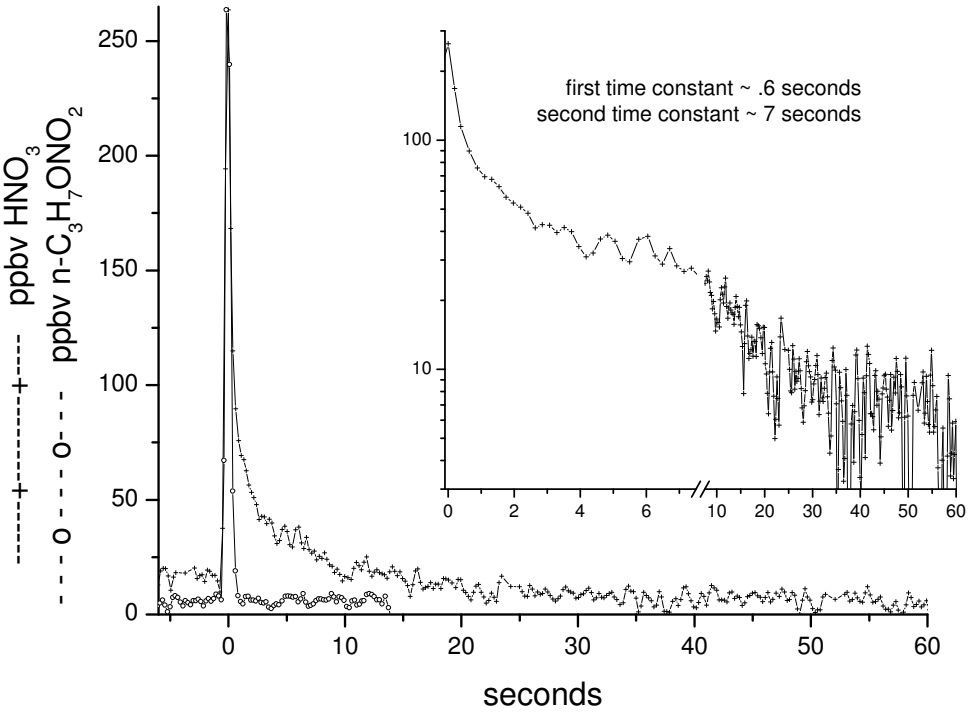

Fig. 2. Response to HNO_3 and n-propyl nitrate spike tests in the laboratory. The inset illustrates the recovery after the HNO_3 spike.

ACPD
6, 2923–2964, 2006

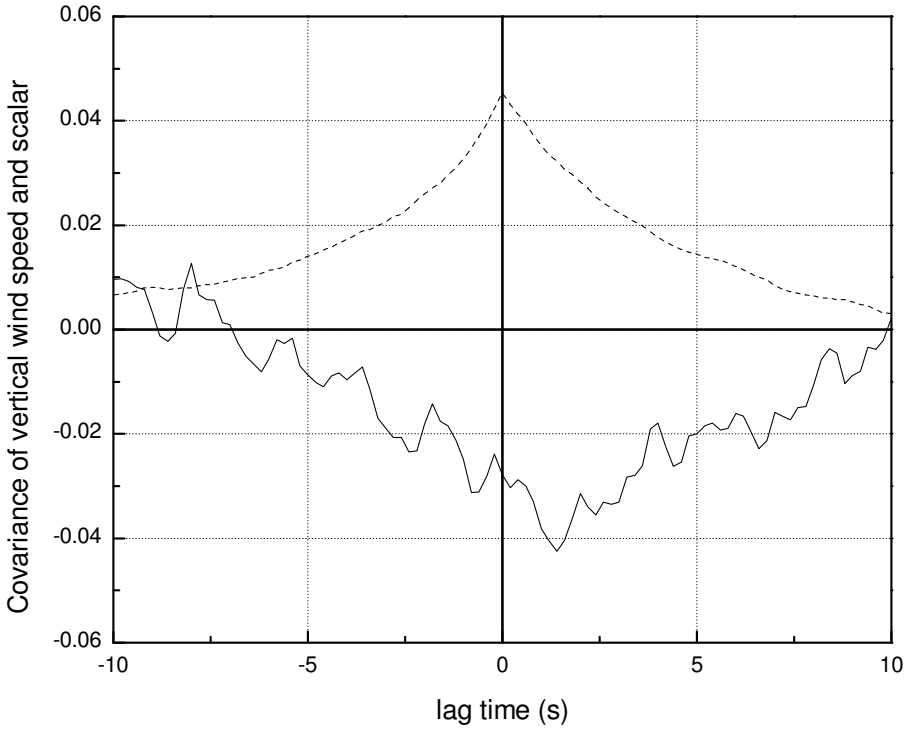

Fig. 3. The lag correlation diagram demonstrates that the covariance (ppb m s^{-1}) for the vertical wind speed and 550°C (ΣNO_{yi}) TD-LIF channel (solid line) maximizes at a lagtime of 2.2 s for this half-hour in the late morning of 17 September 2004. The sensible heat covariance (°C m s^{-1}, divided by 10, dashed line) maximizes at 0 s.

ACPD
6, 2923–2964, 2006

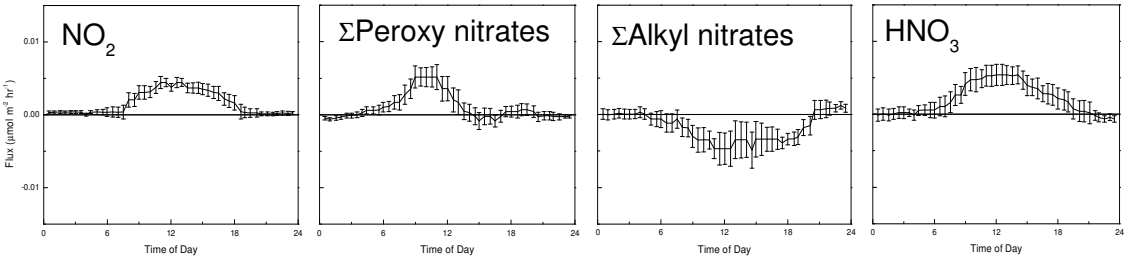

Fig. 4. Average fluxes (running mean with standard error, ppb m s^{-1}) of NO_2, ΣPNs, ΣANs and HNO_3 from the summer (June–August) 2004.

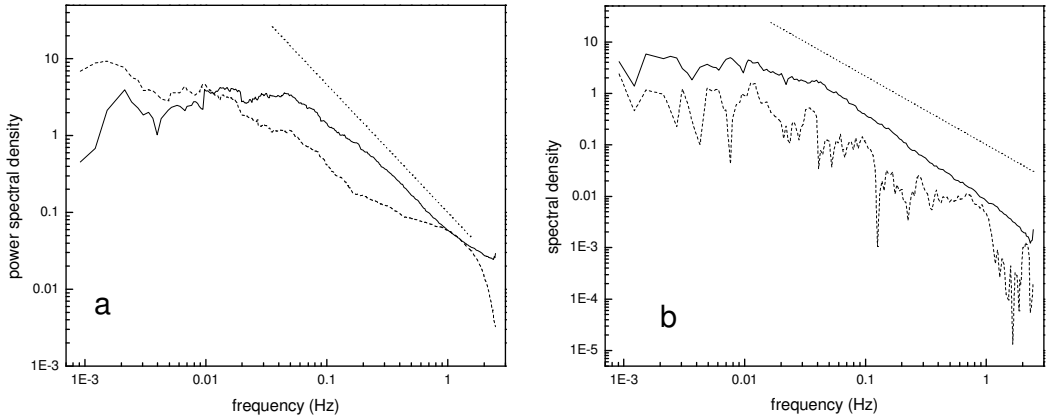

Fig. 5. Power spectrum of vertical wind speed (solid line) and NO_2 (dashed line) observed during a single half hour in the afternoon of 17 September 2004; **(a)** line with a –5/3 slope indicates the presence of an inertial subrange. **(b)** Cospectra of vertical wind speed and temperature (solid line) and vertical wind speed and NO_2 (dashed line) for the same half-hour as (a). A line with a –4/3 slope indicates the presence of an inertial subrange. Note that the power spectra are binned into 500 evenly spaced intervals along the logarithmic frequency axis; cospectra are similarly binned into 200 intervals.

ACPD
6, 2923–2964, 2006

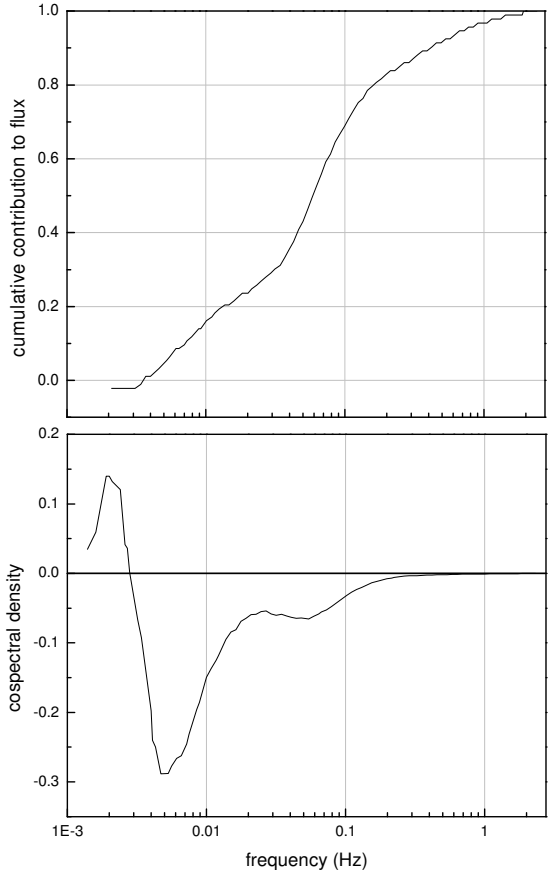

Fig. 6. Averaged semilogarithmic cospectrum **(a)** and normalized cumulative contribution to the flux **(b)** from all daytime data of ΣANs for 1 August–10 August 2004. The cospectrum is binned into 100 evenly spaced intervals along the frequency axis.

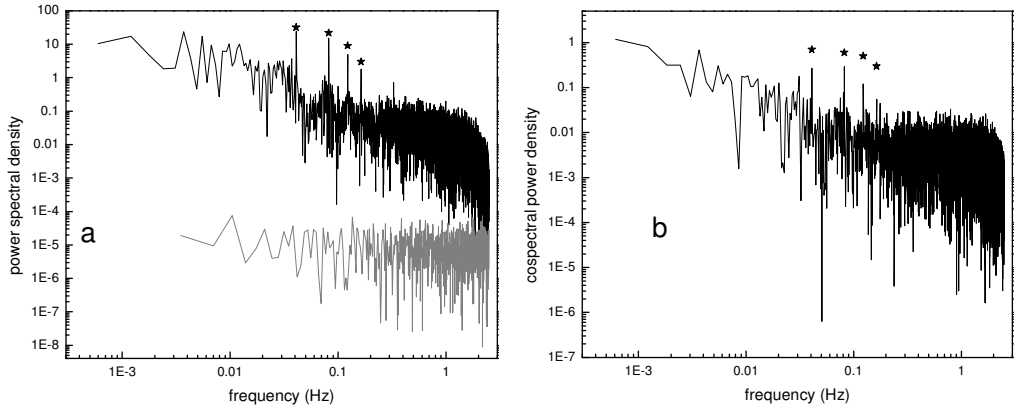

Fig. 7. Unsmoothed power spectra **(a)** of ΣNO_{yi} (black) and instrument noise (grey) for this channel, and cospectrum **(b)** of ΣNO_{yi} and vertical wind speed for a single half hour; stars are at 0.04, 0.08, 0.12, and 0.16 Hz marking the frequency and harmonics of the etalon chop cycle.

ACPD
6, 2923–2964, 2006

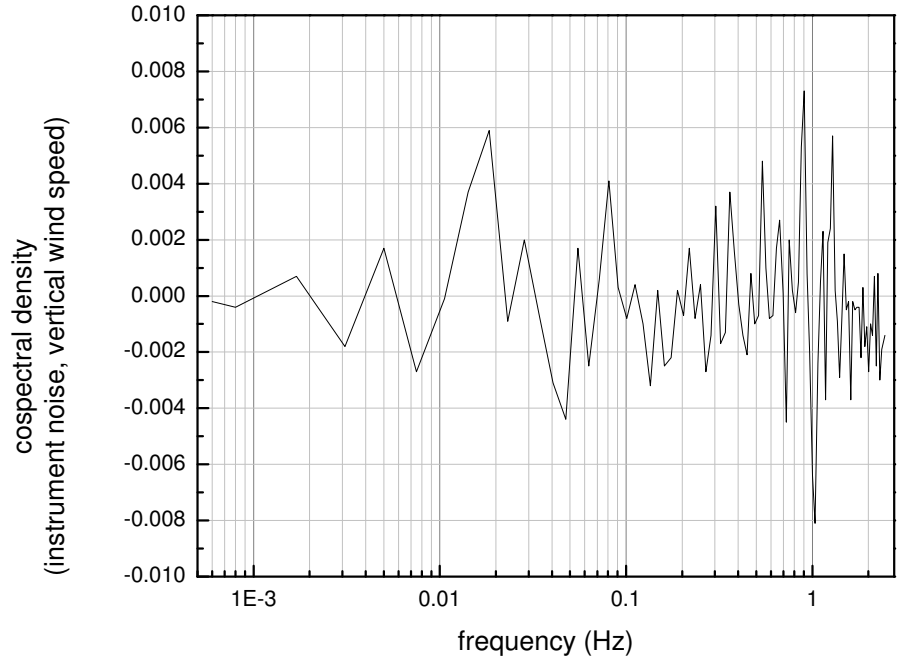

Fig. 8. Cospectrum of instrument noise (zero air measurements) and vertical wind speed, demonstrating the lack of covariance and thus minimal impact of noise on observed fluxes. This cospectrum is binned into 94 evenly spaced intervals along the logarithmic frequency axis.

ACPD
6, 2923–2964, 2006

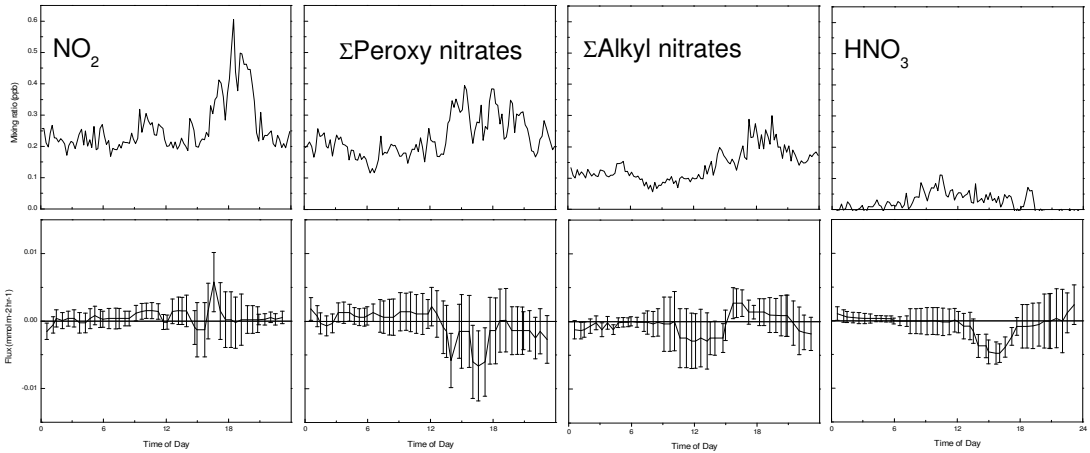

Fig. 9. Average mixing ratios (ppb, upper panels) and fluxes (running mean with standard error, ppb m s^{-1}, lower panels) of HNO_3, Σalkyl nitrates, Σperoxy nitrates, and NO_2 for winter (1 January–31 March 2005).

ACPD
6, 2923–2964, 2006

EGU